Optimal tuning of a Brownian information engine operating in a nonequilibrium steady state

Govind Paneru,[1] Dong Yun Lee,[1] Jong-Min Park,[2] Jin Tae Park,[1,3] Jae Dong Noh,[2] and Hyuk Kyu Pak[1,3,*]

[1]*Center for Soft and Living Matter, Institute for Basic Science, Ulsan 44919, Republic of Korea*

[2]*Department of Physics, University of Seoul, Seoul 02504, Republic of Korea*

[3]*Department of Physics, Ulsan National Institute of Science and Technology, Ulsan 44919, Republic of Korea*

(Received 3 April 2018; revised manuscript received 7 September 2018; published 16 November 2018)

A Brownian information engine can induce directed motion of a Brownian particle in a single heat bath at constant temperature by extracting work from the information about the microscopic state of the particle, and serves as a model for artificial and biological submicron scale engines. Much of the experimental studies to date are limited to the realization of an information engine where the initial state of the system is in thermal equilibrium; however, most of the biological and artificial motors operate far from equilibrium. Here, we realize a cyclic information engine operating in a nonequilibrium steady state consisting of a Brownian particle in an optical trap and investigate the optimal operating conditions for maximum work, power, and efficiency. The performance of our information engine depends on the cycle period τ and the distance x_f that the trap center is shifted with respect to the reference distance x_m. We found that the extracted work increases with increasing τ and is maximum when τ reaches infinity and $x_f = 2x_m$, while the extracted power is maximum at finite τ for $x_f \geqslant x_m$ and when τ approaches zero for $x_f < x_m$. By measuring the steady-state information, we have also measured the efficiency at maximum power.

DOI: 10.1103/PhysRevE.98.052119

I. INTRODUCTION

The idea of extracting work from a single heat bath dates back to thought experiments such as Maxwell's demon [1] and Szilard's engine [2]. In these experiments the extraction of work from a single heat bath decreases the entropy of the system, which supposedly violates the second law of thermodynamics. This paradox was resolved apparently by elucidating the link between information acquired by the demon and thermodynamic entropy [3–5]. However, the quantitative relation between information and thermodynamics was derived by Sagawa and Ueda by introducing the generalized second law of thermodynamics [6–8], which shows that the decrease in thermodynamic entropy is balanced by the amount of information gained by the measurement. Moreover, by utilizing the information obtained by the measurements, we can extract work that cannot exceed the sum of the free energy difference and the available information. Various theoretical models for an information engine the initial state of which is in thermal equilibrium have been investigated for classical [9–11] and quantum [6,12–14] systems, and are validated by recent experiments on Brownian [15–19] and electronic systems [20–23]. For example, Koski *et al.* [20] realized a Szilard engine by performing feedback control on a single electron box and measured the average extracted work per cycle to be ∼0.75 times Landauer's limit [4]. Recently, Paneru *et al.* realized a lossless Brownian information engine that converts nearly all available information into work extraction via an error-free measurement and feedback control, thereby achieving the equality of the generalized second law [17]. Apart from these single temperature bath feedback driven information engines, many non-feedback-driven stochastic Brownian heat engines operating between two heat baths have also been studied recently [24–27]. The experimental realization of these submicron scale engines has improved our understanding of stochastic and information thermodynamics significantly.

The above mentioned studies where the initial state of the system is in thermal equilibrium are still not sufficient to explain the thermodynamics of many biological motors [28] that operate with a finite cycle period where the initial state of the system may not be in thermal equilibrium. To this end, many theoretical works on an information engine operating with a finite cycle period and arbitrary initial state have been reported [29–35]. However, the parametric study of a Brownian information engine operating in a nonequilibrium steady state has been done rarely because of the difficulty in finding the steady-state probability distribution, especially for the case of asymmetric feedback for which the probability distribution function for a finite cycle period is non-Gaussian [35]. Here, we report on the experimental realization of such a cyclic information engine operating in a nonequilibrium steady state where measurement and subsequent feedback control are repeated with a finite cycle time in order to find the optimal condition for maximum work, power, and efficiency. Apart from maximum efficiency, we are interested in measuring the efficiency at maximum power. The determination of efficiency at maximum power has been studied extensively for stochastic two temperature bath heat engines [24,25,36,37]; however, no experimental studies have been done so far in this direction for a single temperature bath Brownian information engine.

Our Brownian information engine consists of a colloidal particle trapped in a harmonic potential generated by optical tweezers and subjected to periodic feedback control. Each engine cycle consists of three processes: acquiring

*hyuk.k.pak@gmail.com

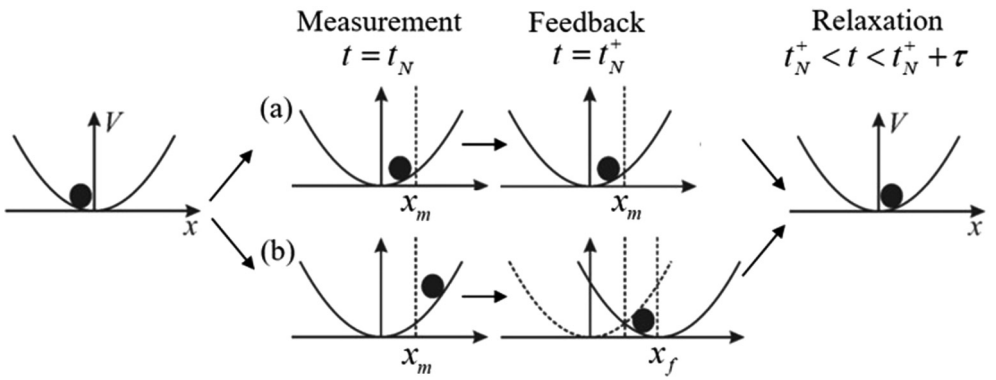

FIG. 1. Illustration of the Nth feedback cycle. A particle is trapped in a harmonic potential generated by an optical trap. We set a line at x_m and measure the particle position at t_N. (a) If the particle is to the left of x_m, we do nothing. (b) If the particle is to the right of x_m, we instantaneously shift the potential center to x_f. After that, the particle relaxes for time τ and another cycle is repeated. By shifting the potential center, the engine extracts work equal to the change in potential energy ΔV.

information about the position of the particle by performing a high precision measurement of the particle position, ultrafast modulation of the trap center, and relaxation of the particle for time τ. Repeating this process for a large number of measurement-feedback-relaxation cycles, the engine can induce one-way transport of the particle, thereby extracting work from the random thermal fluctuations of the surrounding heat bath. We found the optimal operating condition of the engine in a steady state for maximum work and power. The extracted work is maximized when $\tau \to \infty$, while, depending on the feedback control parameters, the extracted power is maximum either at finite τ or in the limit $\tau \to 0$. By measuring the information in a steady state, we also measured the efficiency of this engine and, for the first time, found the optimal conditions for maximum efficiency at maximum power.

II. RESULTS

We consider one dimensional motion of a Brownian particle in a heat bath of temperature $T = (k_B\beta)^{-1}$. As shown in Fig. 1, the particle is trapped in a harmonic potential $V(x_B, X(t)) = (k/2)[x_B - X(t)]^2 \equiv 1/2kx^2$, where x_B is the position of the particle, $X(t)$ denotes the time-dependent potential center, k is the trap stiffness, and $x \equiv x_B - X(t)$ is the relative position of the particle with respective to the potential center. Neglecting the inertial force, the dynamics of the particle during the relaxation can be described by the overdamped Langevin equation [38,39] with the characteristic relaxation time $\tau_R = \gamma/k$, where γ is the dissipation coefficient.

The information engine in this experiment is designed to measure the particle position and modulate the potential center depending on the measurement outcome. Each engine cycle consists of a nearly error-free measurement of the particle position that is followed by instantaneous feedback control and relaxation (see Fig. 1). We set a reference line at x_m and measure the particle position at $t = 0$ and determine which side of the reference line the particle is located at. If the particle is found on the left of x_m, we do nothing, whereas, if the particle is found on the right of x_m, the potential center is instantaneously shifted (keeping the stiffness constant) to x_f. By shifting the potential center, the work performed on the system W is equal to the change in potential energy ΔV. After each feedback operation, the particle evolves in time with a fixed trap center until the next cycle begins. During this relaxation part, the particle exchanges heat with the heat bath without work extraction. Therefore, each engine cycle is characterized by three parameters: the setting distance x_m, the potential center moving distance x_f, and the time period τ for relaxation. Note that the measurement and the feedback control are ideally instantaneous, and the cycle period is $\sim\tau$. In this paper, we fix x_m and vary x_f for different τ in order to find an optimal choice of the parameter values under which the average extracted work or power is maximum.

For the overdamped system, the kinetic energy of the particle can be neglected. According to Ref. [40], the incremental change in potential energy can be converted to work and heat within the switching time. In this experiment, we use an acoustic optical deflector (AOD) to shift the potential center. The switching time for the AOD is about 20 μs. This time is very short in comparison to the characteristic relaxation time $\tau_R = \gamma/k \sim 3$ ms, but sufficiently larger than the momentum relaxation time $\tau_p = m/\gamma \sim 0.2\,\mu$s for the current setup. Hence, in this very short time scale of the overdamped limit, the position of the particle cannot be far from its previous position [41], so we can neglect the heat production during the feedback process. The extracted work $-W(x; t_N)$ for the Nth cycle when the particle is measured at the relative position x is then given by $-W(x; t_N) = V(x_B, X(t_N)) - V(x_B, X(t_N^+)) = \frac{1}{2}kx^2 - \frac{1}{2}k(x - x_f)^2$ when $x \geqslant x_m$, and $-W(x; t_N) = 0$ otherwise ($x < x_m$). Here, $t_N = N\tau$ is the time for the Nth measurement, and t_N^+ stands for the time right after the feedback.

If the process is repeated periodically where a large number of feedback cycles is allowed, the system goes to a steady state. Then, the average extracted work per cycle in the steady state is given by

$$\langle -W\rangle_{\rm ss} = -\int_{x_m}^{\infty} W(x; t_N)\, p_{\rm ss}(x)\, dx = \frac{1}{2}k\int_{x_m}^{\infty} \left(2xx_f - x_f^2\right) p_{\rm ss}(x)\, dx, \qquad (1)$$

where $p_{ss}(x)$ is the steady-state probability distribution of the particle position at the measurement moments and $\langle\cdots\rangle_{ss}$ denotes the steady-state ensemble average. The integration in Eq. (1) begins at x_m because we can extract work only when $x \geqslant x_m$. The probability of finding the particle on the right of x_m is given by $p_R = \int_{x_m}^{\infty} p_{ss}(x)dx$. Then, the expression for $\langle -W\rangle_{ss}$ takes the following form:

$$\langle -W\rangle_{ss} = \tfrac{1}{2}k\left(2\langle x\rangle_{ss}x_f - x_f^2\right)p_R, \tag{2}$$

where $\langle x\rangle_{ss} = \frac{1}{p_R}\int_{x_m}^{\infty} x\,p_{ss}(x)dx$ is the conditional mean position of the particle given that $x \geqslant x_m$.In the limit $\tau \to \infty$, the system relaxes to the equilibrium state irrespective of the measurement and feedback control. As a result, $p_{ss}(x)$ follows the equilibrium Boltzmann distribution $p_{ss}(x) = (2\pi\sigma^2)^{-1/2}\exp(-x^2/2\sigma^2)$, with a variance $\sigma^2 = (\beta k)^{-1}$. Using this $p_{ss}(x)$, we obtain an expression for $\langle -W\rangle_{ss}$ in the limit $\tau \to \infty$ as

$$\langle -W\rangle_{ss} = kx_f\left[\frac{1}{\sqrt{2\pi\beta k}}\exp\left(-\frac{1}{2}\beta k x_m^2\right) - \frac{x_f}{4}\mathrm{erfc}\left(\sqrt{\frac{\beta k}{2}}x_m\right)\right]. \tag{3}$$

A. Experimental setup

The details of the experimental setup are described in our recently published work [17] and in Fig. 2. Briefly, a laser with a 1064-nm wavelength is used for trapping the particle. The laser is fed to an AOD (Isomet, LS110A-XY) via an isolator and a beam expander. The AOD is controlled via an analog voltage controlled rf synthesizer driver (Isomet, D331-BS). The AOD is properly mounted at the back focal plane of the objective lens so that k is essentially constant while shifting the potential center. A second laser with a 980-nm wavelength is used for tracking the particle position. A quadrant photodiode (QPD) (Hamamatsu, S5980) is used to detect the particle position. The electrical signal from the QPD is preamplified by a signal amplifier (On-Trak Photonics Inc., OT-301) and sampled at every τ with a field-programmable gate array (FPGA) data acquisition card. Our system is capable of measuring the particle position with a high spatial accuracy of 1 nm [17]. The sample cell consists of a highly diluted solution of 2.0-μm-diameter polystyrene particles suspended in deionized water. All experiments were carried out at 293 ± 0.1 K. The parameters of the trap were calibrated by fitting the probability distribution of the particle position in a thermal equilibrium without a feedback process to the Boltzmann distribution $P(x) = (2\pi\sigma^2)^{-1/2}\exp(-x^2/2\sigma^2)$, and we obtain the standard deviation $\sigma = 25$ nm. The trap stiffness was then obtained by using the relation $k = k_BT/\sigma^2$ and was found to be 6.47 pN/μm [17,42]. The characteristic relaxation time for the current setup is equal $\tau_R = \gamma/k = 3$ms. In comparison to the particle position distribution with $\sigma = 25$ nm, the measurement error of 1 nm is negligible. Hence, we assume our system is capable of performing nearly error-free measurements.

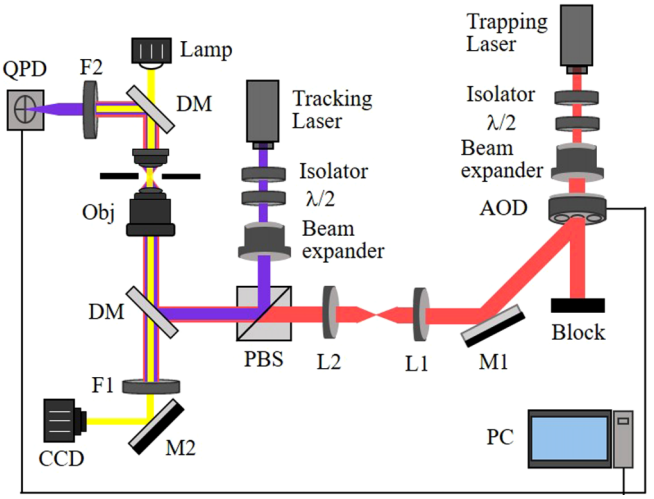

FIG. 2. Schematics of the optical tweezers setup with feedback control system. The FPGA board (connected inside the personal computer, PC) generates a bias voltage that corresponds to the initial position of the trapping laser center. This voltage is applied to the AOD and a highly focused laser beam (optical trap) is created at the sample plane of the microscope. A polystyrene bead is trapped by this laser beam. The QPD, mounted at the back focal plane of the condenser, performs a nearly error-free measurement of the particle position with the help of the tracking laser beam (of very low laser power). The measurement outcome is sent to the FPGA board. The FPGA generates the updated voltage that corresponds to the shift of the trap (trapping laser) center. This voltage is sent to the AOD and the trap center is updated. M1, M2: mirror. L1, L2: lens. DM: dichroic mirror. PBS: polarizing beam splitter. F1, F2: filter. $\lambda/2$: half waveplate.

B. Feedback control design

The FPGA board generates the initial bias voltage that corresponds to the initial position of the potential center (the trapping laser beam center). This bias voltage is applied to the AOD via an rf synthesizer, thereby creating an optical trap at the sample plane of the microscope. Our Brownian information engine consists of a polystyrene particle that is trapped by the laser $\sim$20 μm above the bottom of the sample cell. The information engine operates by measuring the position of the Brownian particle with respect to the trap center using the QPD. If the particle is found on the left of x_m, nothing is changed and another measurement is repeated after time τ. If the particle is found on the right of x_m, the FPGA board generates an updated bias voltage that corresponds to the shift of the potential center by x_f. The decision whether to update the bias voltage and shift the potential center is taken in 20 μs. After shifting the potential center, we again wait for time τ, during which the particle relaxes in the updated potential center, and another engine cycle is repeated. The number of feedback cycles is limited by the working area of the QPD and the linear scan range of the AOD up to which the trap stiffness remains constant, which is about 0.5 μm for our current setup.

In our recent paper, the optimal value of x_m for maximum work extraction was found to be $x_m \sim 0.6\sigma$ [17]. Hence, in this paper we fix $x_m \sim 0.6\sigma$ and vary x_f and τ in order

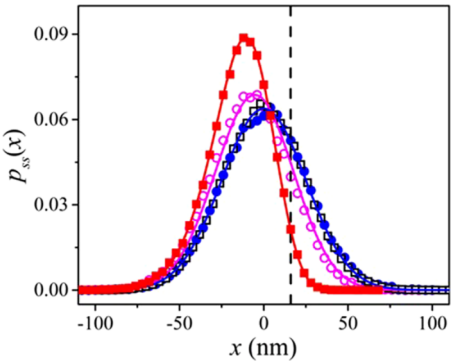

FIG. 3. Steady-state probability distribution of the particle position for different τ with $x_m = 16$ nm and $x_f = 32$ nm. The red solid squares, magenta open circles, and blue solid circles correspond to $\tau = 0.2$, 2.0, and 20.0 ms, respectively. The distribution measured for $\tau = 20$ ms follows the equilibrium distribution obtained without feedback control (see black open squares). The solid curves represent the analytical results obtained by using Eq. (A8) in the Appendix. The dashed vertical line corresponds to $x_m = 16$ nm.

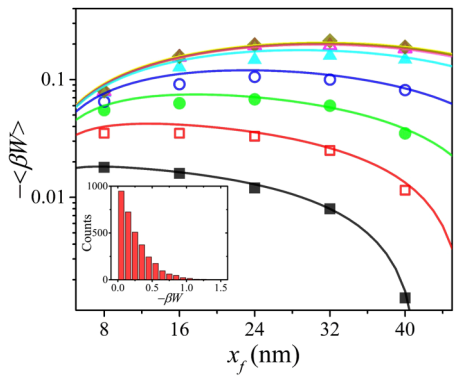

FIG. 4. τ Average extracted work per engine cycle as a function of x_f for seven different τ with x_m fixed at 16 nm. The black solid squares, red open squares, green solid circles, blue open circles, cyan solid triangles, magenta open triangles, and dark yellow solid diamonds correspond to the average work values for $\tau = 0.2$, 0.5, 1.0, 2.0, 5.0, 10.0, and 20.0 ms, respectively. The solid curves are plots of Eq. (A9) in the Appendix. The topmost yellow solid curve is the plot of Eq. (3). Inset: Histogram of the extracted work, $-\beta W = \beta[V(x) - V(x - x_f)]$ for $x_m = 16$ nm, $\tau = 0.2$ ms, and $x_f = 2x_m$.

to find the optimal condition for maximum work and power extraction. Figure 3 shows the experimentally measured steady-state probability distribution $p_{\rm ss}(x)$ of the particle position for different τ with $x_m = 16$ nm ($x_m \sim 0.6\sigma$) and $x_f = 32$ nm. For small τ, $p_{\rm ss}(x)$ is a highly asymmetric function which spreads out to the right of x_m on increasing τ and matches with the equilibrium distribution for $\tau \gtrsim 5\tau_R$. Note that only the points on the right of x_m contribute to the extracted work. Furthermore, the experimentally measured $p_{\rm ss}(x)$ fits well with the solid curves that were obtained by plotting the analytical results in Eq. (A8) presented in the Appendix that were derived by the method used in Ref. [35].

The experimentally measured average extracted work per engine cycle in the steady state $\langle -\beta W\rangle$ as a function of x_f for seven different τ with x_m fixed at 16 nm is shown in Fig. 4. For $x_f > 0$, $\langle -\beta W\rangle$ increases with increasing τ and saturates when the system relaxes fully, corresponding to $\tau \gtrsim 5\tau_R$. The global maximum of $\langle -\beta W\rangle$ is obtained when $x_f = 2x_m$ and $\tau \gtrsim 5\tau_R$. From Ref. [35] we note that, given the particle position $x > x_m$, the extracted work is maximum if the particle is shifted to the center of the potential (in the relative frame of reference). Thus, x_f should be taken as the conditional mean position of the particle $\langle x\rangle_{\rm ss}$, which is $\sim 1.2\sigma$ when $x_m \sim 0.6\sigma$. This is the reason why the global maximum of $\langle -\beta W\rangle$ is at $x_f = 2x_m$. For $\tau \leqslant \tau_R$, the optimal value of x_f for the maximum $\langle -\beta W\rangle$ decreases and goes to zero as $\tau \to 0$. The solid curves obtained by plotting Eq. (A9) in the Appendix fit well with the experimentally measured $\langle -\beta W\rangle$ and also fit to the theoretical curve (yellow solid curve) in Eq. (3). It is worth mentioning that in comparison to the work extraction by always moving the trap center in one direction (without feedback), where the extracted work $-\beta W$ is not always positive [43], our feedback controlled information engine is capable of extracting positive work for all cycles (see the inset of Fig. 4). Hence, the feedback control enhances the magnitude of the average work extraction significantly.

Figures 5(a) and 5(b) show the plot of the experimentally measured average extracted power $\langle \beta P\rangle = \langle -\beta W\rangle/\tau$ as a function of τ and x_f, respectively, when x_m is fixed at 16 nm. We found that the global maximum of $\langle \beta P\rangle$ is obtained when $\tau \ll \tau_R$ and $x_f \ll x_m$. Our finding is in agreement with the recent theoretically realized Brownian information engine [35], which shows that the extracted power is maximum when $\tau \to 0$ and $x_f \to 0$. However, for $x_f \geqslant x_m$, $\langle \beta P\rangle$ is found to be maximum at finite τ. The solid curves are the plots of $\langle -\beta W\rangle_{\rm ss}/\tau$ using Eq. (A9) in the Appendix and fit well with the experimentally measured power.

Another quantity of interest is the efficiency of the Brownian information engine in the steady state, which is defined as $\eta = \langle -\beta W\rangle_{\rm ss}/\langle I\rangle$, where $\langle I\rangle$ is the mean information acquired through the measurement [32]. Considering there is negligible error in the estimation of the particle position in this experiment, $\langle I\rangle$ is given by Shannon information [44] (see also Ref. [17]). In the current feedback scheme, each engine cycle has two discrete measurement outcomes: with probability p_R the particle is found on the right of x_m and with probability $1 - p_R$ the particle is found on the left of x_m. Thus, the acquired information is simply given by $\langle I\rangle = -p_R \ln p_R - (1 - p_R)\ln(1 - p_R)$. Figure 6 shows the plot of the engine's efficiency measured as a function of x_f for different τ. We found that, for a given x_f, efficiency increases with increasing τ. The maximum efficiency of $\sim$35% was obtained when $x_f = 2x_m$ and $\tau \gtrsim 5\tau_R$. Our experimentally measured efficiency fits well with the solid curves obtained by using Eq. (A11) in the Appendix. The nearly error-free position measurement and instantaneous shift of the potential center allow us to extract the maximum amount of information. However, some part of the information gain is not fully utilized during the relaxation part of the engine cycle. Also, the acquired information is useless for work extraction when the particle is found on the left of x_m. These are the two reasons why the measured efficiency is less than the unity. Considering the true available information, we expect that this

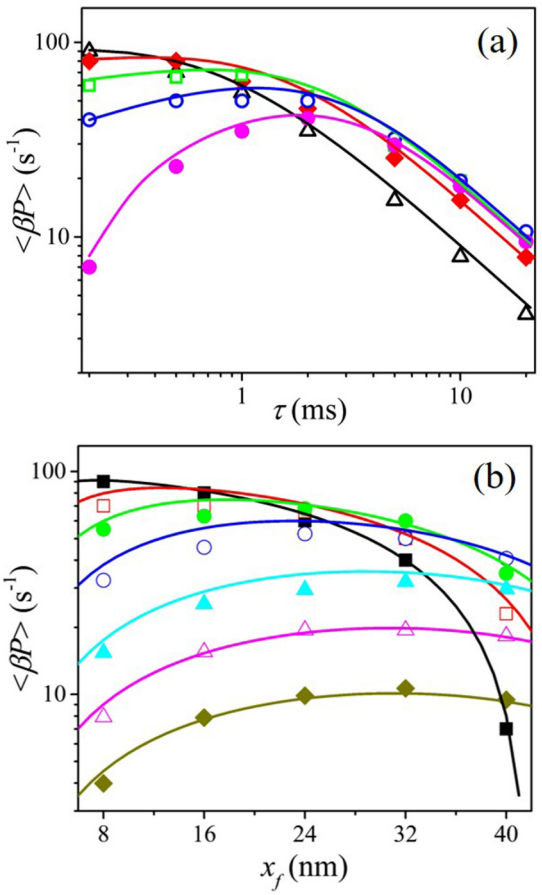

FIG. 5. (a) Average extracted power as a function of τ for different x_f with x_m fixed at 16 nm. The black open triangles, red solid squares, green open squares, blue solid circles, and magenta solid circles correspond to the average power for $x_f = 8$, 16, 24, 32, and 40 nm, respectively. (b) Average extracted power as a function of x_f for different τ with x_m fixed at 16 nm. The black solid squares, red open squares, green solid circles, blue open circles, cyan solid triangles, magenta open triangles, and dark yellow solid diamonds correspond to the average power for $\tau = 0.2$, 0.5, 1.0, 2.0, 5.0, 10.0, and 20.0 ms, respectively. The solid curves in both panels (a) and (b) are the plots of $\langle -\beta W \rangle_{ss}/\tau$ using Eq. (A9) in the Appendix.

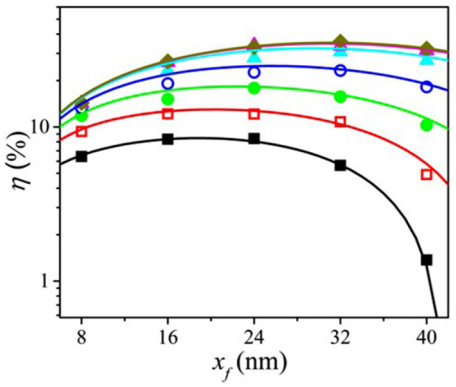

FIG. 6. Plot of the engine's efficiency as a function of x_f for different τ with x_m fixed at 16 nm. The black solid squares, red open squares, green solid circles, blue open circles, cyan solid triangles, magenta solid triangles, and dark yellow solid diamonds correspond to the efficiency for $\tau = 0.2$, 0.5, 1.0, 2.0, 5.0, 10.0, and 20.0 ms, respectively. The solid curves are the plots of Eq. (A11) in the Appendix.

engine may achieve the upper bound of the generalized second law [10,17]. We also measured the efficiency of this engine at maximum power and found that for $x_f < x_m$ the engine has vanishing efficiency at maximum power (which is for $x_f \sim 0$ and $\tau \sim 0$). However, for $x_f \geqslant x_m$, the efficiency at maximum power is found to be highest (equal to ~19%) for $x_f = 2.5x_m$ and near $\tau_R (\tau = 2\,\text{ms})$.

III. CONCLUSIONS

In conclusion, we studied the cyclic Brownian information engine consisting of a colloidal particle trapped in a harmonic potential. Each engine cycle consists of three steps: particle position measurement, shifting of the potential center based on measurement outcome, and relaxation. Each process is characterized by three parameters: x_m for measurement, x_f for feedback, and τ for relaxation. We fix x_m and change x_f for different τ in order to find an optimal condition for maximum extracted work or power. We found that the global maximum of extracted work per engine cycle is obtained when the system is fully relaxed and $x_f = 2x_m$. On the other hand, the global maximum of extracted power is obtained when both x_f and τ approach zero. For $x_f \geqslant x_m$, the extracted power is maximum at finite τ , although the global maximum of power is obtained when $\tau \to 0$; however, it is somewhat useless because in this case both the extracted work and the efficiency are vanishing. On the other hand, the extracted work and the efficiency are maximum when the system is fully relaxed for which the extracted power is vanishing. On the basis of these observations, the optimized parameters for maximum power extraction with nonzero work and efficiency are $x_m \sim 0.6\sigma$, $x_f \sim 2x_m$, and $\tau \sim \tau_R$. Since our current setup is capable of performing high precision measurements and ultrafast feedback control, this should allow one to probe how information is transformed in microscale and nanoscale systems in a nonequilibrium steady state. Our paper will also assist in design and understanding of efficient synthetic as well as biological stochastic motors.

ACKNOWLEDGMENTS

This work was supported by the Korean government under Grants No. IBS-R020-D1 (H.K.P.) and No. 2016R1A2B2013972 (J.D.N.).

G.P. and D.Y.L. contributed equally to this work.

APPENDIX: THEORY

Here, we explain the method to find the analytic results presented in the main text. More details of the derivations are found in Ref. [35].

As the engine repeats the cycle, the probability density for the relative position x converges to the time-periodic state. We focus on the probability density after the relaxation process just before the next measurement and feedback process in

the time-periodic regime. It will be denoted as $p_{\rm ss}(x)$ By definition, $p_{\rm ss}(x)$ should be invariant under the measurement and feedback process followed by the relaxation process for the time interval τ. The invariance property allows us to find $p_{\rm ss}(x)$.

It is convenient to consider a series expansion

$$p_{\rm ss}(x) = \sum_{n=0}^{\infty} c_n \phi_n(x), \tag{A1}$$

where c_n are the expansion coefficients and $\phi_n(x) = H_n\frac{x}{\sqrt{2}\sigma}e^{-x^2/2\sigma^2}$ with the Hermite polynomial $H_n(x)$ of degree n and the standard deviation σ defined in the main text. With this expansion, the invariance condition of $p_{\rm ss}(x)$ under the engine cycle takes the form of the self-consistent equation [35]

$$\boldsymbol{c} = \mathbf{W}(\mathbf{I} + \mathbf{F})\boldsymbol{c} \tag{A2}$$

for the column vector $\boldsymbol{c} = (c_0,\ c_1, c_2, \ldots)^T = (c_0,\ \tilde{\boldsymbol{c}})^T$ for the expansion coefficients, where $\mathbf{I}$ is the identity matrix and the matrices $\mathbf{W}$ and $\mathbf{F}$ are in a block form:

$$\mathbf{W} = \begin{pmatrix} 1 & 0 \\ 0 & \tilde{\mathbf{W}} \end{pmatrix},\quad \mathbf{F} = \begin{pmatrix} 0 & 0 \\ \tilde{\boldsymbol{f}} & \tilde{\mathbf{F}} \end{pmatrix}. \tag{A3}$$

The submatrices $\tilde{\mathbf{W}}$ and $\tilde{\mathbf{F}}$ and the column vector $\tilde{\boldsymbol{f}}$ have the elements

$$\tilde{W}_{ab} = e^{-a\frac{\tau}{\tau_R}}\delta_{ab}, \tag{A4}$$

$$\tilde{F}_{ab} = \frac{1}{\sqrt{2\pi}\sigma 2^a a!}\sum_{k=0}^{a-1}\binom{a}{k}\left(-\frac{\sqrt{2}x_f}{\sigma}\right)^{a-k} \times \int_{x_m}^{\infty} H_k\left(\frac{x}{\sqrt{2}\sigma}\right)\phi_b(x)dx, \tag{A5}$$

$$\tilde{f}_a = \frac{1}{\sqrt{2\pi}\sigma 2^a a!}\sum_{k=0}^{a-1}\binom{a}{k}\left(-\frac{\sqrt{2}x_f}{\sigma}\right)^{a-k} \times \int_{x_m}^{\infty} H_k\left(\frac{x}{\sqrt{2}\sigma}\right)e^{-\frac{x^2}{2\sigma^2}}dx, \tag{A6}$$

for positive integers a and b with the relaxation time τ_R in the main text. The value of $c_0 = 1/(\sqrt{2\pi}\sigma)$ is fixed by the normalization condition $\int dx p_{\rm ss}(x) = 1$.

The self-consistent equation yields

$$\tilde{\boldsymbol{c}} = \frac{1}{\sqrt{2\pi}\sigma}\tilde{\mathbf{W}}[\mathbf{I} - (\mathbf{I} + \tilde{\mathbf{F}})\tilde{\mathbf{W}}]^{-1}\tilde{\boldsymbol{f}}. \tag{A7}$$

This requires one to invert the infinite dimensional matrix, which is intractable. Nevertheless, we can find an approximate solution by truncating the series in Eq. (A1) keeping only terms with $n = 0,\ \ldots,\ L$. Under the truncation, $\mathbf{I}$, $\tilde{\mathbf{W}}$, and $\tilde{\mathbf{F}}$ become $L \times L$ matrices and $\tilde{\boldsymbol{f}}$ becomes an L-dimensional column vector. Since $c_n \sim e^{-n\tau/\tau_R}$ from Eq. (A7), the error due to the truncation is of the order of $e^{-(L+1)\tau/\tau_R}$ [35]. Thus, one can increase the accuracy by choosing a large enough value of L.

With the experimental parameters $\tau_R = 3\,\text{ms}$, $\sigma = 25\,\text{nm}$, and $x_m = 16\,\text{nm}$, we evaluate the approximate solutions $c_1^*,\ c_2^*,\ \ldots,\ c_L^*$ up to $L = 27$ as varying x_f and τ. Hereafter, the superscript $*$ stands for the approximate solution from the truncation method. For those parameters, numerical errors are negligible with $L = 27$. Once the coefficients c_n^* are evaluated, the thermodynamic quantities of interest can be easily obtained. First, the steady-state probability density is given by

$$p_{\rm ss}^*(x) = \sum_{n=0}^{L} c_n^*\phi_n(x). \tag{A8}$$

Thanks to the orthogonality of the Hermite functions, the average extracted work is expressed as a simple form [35], that is,

$$-\beta\langle W_{\rm ss}^*\rangle = -\sqrt{8\pi}\sigma(e^{2\frac{\tau}{\tau_R}} - 1)c_2^*. \tag{A9}$$

The average power is then obtained by the average work divided by the cycle time τ. Using Eqs. (A2), (A5), and (A6), we also obtain the probability p_R^* that the particle is on the right side of x_m in the measurement process:

$$p_R^* = \sum_{n=0}^{L} c_n^*\int_{x_m}^{\infty} dx\phi_n(x) = -\frac{\sqrt{4\pi}\sigma^2}{x_f}(e^{\tau/\tau_R} - 1)c_1^*. \tag{A10}$$

Finally, the efficiency is given by

$$\eta^* = \frac{-\beta\langle W\rangle_{ss}^*}{\langle I\rangle^*} = \frac{\beta\langle W\rangle_{ss}^*}{p_R^*\ln p_R^* + (1 - p_R^*)\ln(1 - p_R^*)}. \tag{A11}$$

[1] H. S. Leff and A. F. Rex, *Maxwell's Demon 2: Entropy, Classical and Quantum Information, Computing* (Princeton University, Princeton, NJ, 2003).
[2] L. Szilard, Z. Phys. **53**, 840 (1929).
[3] L. Brillouin, J. Appl. Phys. **22**, 334 (1951).
[4] R. Landauer, IBM J. Res. Dev. **5**, 183 (1961).
[5] C. H. Bennett, Int. J. Theor. Phys. **21**, 905 (1982).
[6] T. Sagawa and M. Ueda, Phys. Rev. Lett. **100**, 080403 (2008).
[7] T. Sagawa and M. Ueda, Phys. Rev. Lett. **102**, 250602 (2009).
[8] T. Sagawa and M. Ueda, Phys. Rev. Lett. **104**, 090602 (2010).
[9] D. Abreu and U. Seifert, Europhys. Lett. **94**, 10001 (2011).
[10] Y. Ashida, K. Funo, Y. Murashita, and M. Ueda, Phys. Rev. E **90**, 052125 (2014).
[11] P. S. Pal, S. Rana, A. Saha, and A. M. Jayannavar, Phys. Rev. E **90**, 022143 (2014).
[12] S. W. Kim, T. Sagawa, S. De Liberato, and M. Ueda, Phys. Rev. Lett. **106**, 070401 (2011).
[13] D. E. Bruschi, M. Perarnau-Llobet, N. Friis, K. V. Hovhannisyan, and M. Huber, Phys. Rev. E **91**, 032118 (2015).

[14] G. John, H. Marcus, R. Arnau, R. Lídia del, and S. Paul, J. Phys. A: Math. Theor. **49**, 143001 (2016).
[15] B. J. Lopez, N. J. Kuwada, E. M. Craig, B. R. Long, and H. Linke, Phys. Rev. Lett. **101**, 220601 (2008).
[16] S. Toyabe, T. Sagawa, M. Ueda, E. Muneyuki, and M. Sano, Nat. Phys. **6**, 988 (2010).
[17] G. Paneru, D. Y. Lee, T. Tlusty, and H. K. Pak, Phys. Rev. Lett. **120**, 020601 (2018).
[18] A. Bérut, A. Arakelyan, A. Petrosyan, S. Ciliberto, R. Dillenschneider, and E. Lutz, Nature (London) **483**, 187 (2012).
[19] Y. Jun, M. Gavrilov, and J. Bechhoefer, Phys. Rev. Lett. **113**, 190601 (2014).
[20] J. V. Koski, V. F. Maisi, J. P. Pekola, and D. V. Averin, Proc. Natl. Acad. Sci. USA **111**, 13786 (2014).
[21] J. V. Koski, V. F. Maisi, T. Sagawa, and J. P. Pekola, Phys. Rev. Lett. **113**, 030601 (2014).
[22] J. V. Koski, A. Kutvonen, I. M. Khaymovich, T. Ala-Nissila, and J. P. Pekola, Phys. Rev. Lett. **115**, 260602 (2015).
[23] A. Kutvonen, J. Koski, and T. Ala-Nissila, Sci. Rep. UK **6**, 21126 (2016).
[24] V. Blickle and C. Bechinger, Nat. Phys. **8**, 143 (2012).
[25] I. A. Martínez, É. Roldán, L. Dinis, D. Petrov, J. M. R. Parrondo, and R. A. Rica, Nat. Phys. **12**, 67 (2015).
[26] S. Krishnamurthy, S. Ghosh, D. Chatterji, R. Ganapathy, and A. K. Sood, Nat. Phys. **12**, 1134 (2016).
[27] M. Serra-Garcia, A. Foehr, M. Molerón, J. Lydon, C. Chong, and C. Daraio, Phys. Rev. Lett. **117**, 010602 (2016).
[28] M. Schliwa and G. Woehlke, Nature (London) **422**, 759 (2003).
[29] M. Esposito and C. V. d. Broeck, Europhys. Lett. **95**, 40004 (2011).
[30] S. Still, D. A. Sivak, A. J. Bell, and G. E. Crooks, Phys. Rev. Lett. **109**, 120604 (2012).
[31] D. Abreu and U. Seifert, Phys. Rev. Lett. **108**, 030601 (2012).
[32] M. Bauer, D. Abreu, and U. Seifert, J. Phys. A: Math. Theor. **45**, 162001 (2012).
[33] J. M. Horowitz, T. Sagawa, and J. M. R. Parrondo, Phys. Rev. Lett. **111**, 010602 (2013).
[34] J. M. R. Parrondo, J. M. Horowitz, and T. Sagawa, Nat. Phys. **11**, 131 (2015).
[35] J.-M. Park, J. S. Lee, and J. D. Noh, Phys. Rev. E **93**, 032146 (2016).
[36] T. Schmiedl and U. Seifert, Europhys. Lett. **81**, 20003 (2008).
[37] Z. C. Tu, J. Phys. A: Math. Theor. **41**, 312003 (2008).
[38] M. C. Wang and G. E. Uhlenbeck, Rev. Mod. Phys. **17**, 323 (1945).
[39] C. M. V. Vliet, *Equilibrium and Non-Equilibrium Statistical Mechanics* (World Scientific, Singapore, 2010).
[40] K. Sekimoto, Prog. Theo. Phys. Suppl. **130**, 17 (1998).
[41] H. Risken, *The Fokker-Planck-Equation: Methods of Solution and Applications* (Springer, Berlin, 1989).
[42] D. Y. Lee, C. Kwon, and H. K. Pak, Phys. Rev. Lett. **114**, 060603 (2015).
[43] A. Imparato, L. Peliti, G. Pesce, G. Rusciano, and A. Sasso, Phys. Rev. E **76**, 050101 (2007).
[44] C. E. Shannon, Bell Syst. Tech. J. **27**, 379 (1948).